Structural and Functional Characterization of CC Chemokine CCL14[†,‡]

Katherine Y. Blain,[§,||,⊥] Witek Kwiatkowski,[§,||] Qinghai Zhao,[§,#,▲] David La Fleur,[#,▲] Chethana Naik,[#,▲] Tae-Wook Chun,[△] Tatiana Tsareva,[#,▲] Palanisamy Kanakaraj,[#,▲] Michael W. Laird,[#,♦] Rutul Shah,[#,▲] Lisa George,[||] Indra Sanyal,[#,▲] Paul A. Moore,[#,■] Borries Demeler,[○] and Senyon Choe*[,||,⊥]

Structural Biology Laboratory, The Salk Institute, La Jolla, California 92037, Division of Biological Sciences, University of California, San Diego, La Jolla, California 92093, Human Genome Sciences Inc., Rockville, Maryland 20850, National Institute of Allergy and Infectious Diseases, National Institutes of Health, Bethesda, Maryland 20892, and Department of Biochemistry, University of Texas Health Science Center, San Antonio, Texas 78229

Received May 15, 2007; Revised Manuscript Received June 11, 2007

ABSTRACT: CC chemokine ligand 14, CCL14, is a human CC chemokine that is of recent interest because of its natural ability, upon proteolytic processing of the first eight NH_2-terminal residues, to bind to and signal through the human immunodeficiency virus type-1 (HIV-1) co-receptor, CC chemokine receptor 5 (CCR5). We report X-ray crystallographic structures of both full-length CCL14 and signaling-active, truncated CCL14 [9−74] determined at 2.23 and 1.8 Å, respectively. Although CCL14 and CCL14 [9−74] differ in their ability to bind CCR5 for biological signaling, we find that the NH_2-terminal eight amino acids (residues 1 through 8) are completely disordered in CCL14 and both show the identical mode of the dimeric assembly characteristic of the CC type chemokine structures. However, analytical ultracentrifugation studies reveal that the CCL14 is stable as a dimer at a concentration as low as 100 nM, whereas CCL14 [9−74] is fully monomeric at the same concentration. By the same method, the equilibrium between monomers of CCL14 [9−74] and higher order oligomers is estimated to be of $EC_{1,4} = 4.98$ μM for monomer−tetramer conversion. The relative instability of CCL14 [9−74] oligomers as compared to CCL14 is also reflected in the K_d's that are estimated by the surface plasmon resonance method to be ∼9.84 and 667 nM for CCL14 and CCL14 [9−74], respectively. This ∼60-fold difference in stability at a physiologically relevant concentration can potentially account for their different signaling ability. Functional data from the activity assays by intracellular calcium flux and inhibition of CCR5-mediated HIV-1 entry show that only CCL14 [9−74] is fully active at these near-physiological concentrations where CCL14 [9−74] is monomeric and CCL14 is dimeric. These results together suggest that the ability of CCL14 [9−74] to monomerize can play a role for cellular activation.

Chemokines (chemotactic cytokines) are small secreted proteins of 8−10 kDa that are widely known for their participation in the immune and inflammatory response systems. Their ability to recruit and activate leukocytes to sites of injury or infection is made possible through the activation of specific seven-transmembrane G protein-coupled receptors (GPCR)[1] (*1*, *2*). Chemokines are generally grouped into the following three subfamilies based on function: "homeostatic", "inflammatory", and "dual function". Homeostatic chemokines are constitutively produced and secreted, whereas inflammatory chemokines are produced when there is a stimulus or during an infection and they cause the migration of leukocytes to the injured or infected site. The subfamily dual function refers to the chemokines which have dual abilities of the first two subfamilies (*3*). Structurally, these chemokines are classified into the following four categories based on the position of the first two cysteine residues: CC, CXC, C, and CX3C (*4*,

[†] This work was supported by National Institutes of Health Grants HD 013527 (S.C.) and RRR022200 (B.D.), National Science Foundation Grant DBI-9974819 (B.D.), and American Heart Association Predoctoral Fellowship 0615005Y (K.Y.B.).

[‡] The atomic coordinates and structure factors (codes 2Q8T and 2Q8R) have been deposited in the Protein Data Bank, Research Collaboratory for Structural Bioinformatics (http://www.rcsb.org/).

* To whom correspondence should be addressed. E-mail: choe@salk.edu.

[§] These authors contributed equally to this work.

[||] The Salk Institute.

[⊥] University of California, San Diego.

[#] Human Genome Sciences Inc.

[▲] Present address: CoGenesys, Inc., 9410 Key West, Rockville, MD 20850.

[△] National Institute of Allergy and Infectious Diseases, NIH.

[♦] Present address: Genentech, Inc., 1 DNA Way, South San Francisco, CA 94080.

[■] Present address: Celera, 45 West Gude Drive, Rockville, MD 20850.

[○] University of Texas Health Science Center.

[1] Abbreviations: AIDS, acquired immune deficiency syndrome; AOP, aminooxypentane; CCL, CC chemokine ligand; CCR, CC chemokine receptor; CD, cluster of differentiation; EC, equilibrium concentration; FLIPR, fluorometric imaging plate reader; GPCR, G protein-coupled receptor; HBSS, Hank's balanced salt solution; HIV, human immunodeficiency virus; IL-8, interleukin-8; k_{on}, association rate parameter; k_{off}, dissociation rate parameter; M-tropic, macrophage tropic; MCP, monocyte chemoattractant protein; MIP, macrophage inflammatory protein; NMR, nuclear magnetic resonance; PBMC, peripheral blood mononuclear cells; RANTES, regulated on activation normal T cell expressed and secreted; TCL-tropic, T cell line-tropic.

10.1021/bi700936w CCC: $37.00
Published on Web 08/11/2007

5). Currently 28 mammalian CC chemokines have been discovered, with 25 of these found in humans, making the CC chemokines the largest subfamily (*6*). The CXC chemokines platelet factor 4 (CXCL4) (*7*) and interleukin-8 (CXCL8) (*8*−*10*) were the first chemokines for which a three-dimensional structure was solved. Currently, the structures of several chemokines have been elucidated through the methods of both NMR and X-ray crystallography. These studies revealed that chemokines share a common structural scaffold consisting of three antiparallel β-strands and a COOH-terminal α-helix (*11*), but they also showed dissimilarities in the mode of assembly into dimers among different subfamilies. Within the same subfamily, the mode of dimeric assembly is identical.

Due to their role in the immune response, chemokines have been linked to the regulation of many different immunological disorders such as asthma (*12*), arteriosclerosis (*13*), and rheumatoid arthritis (*14*, *15*). Pertaining further medically is the role of certain chemokines to acquired immune deficiency syndrome (AIDS). HIV-1 initiates infection of target cells by fusion of both the viral and target cell membranes. This action is mediated by the binding of the viral envelope glycoprotein (Env) and a CD4 receptor on human target cells. Critical to the efficient infection is the presence of a coreceptor. The importance of the coreceptor provided the explanation underlying HIV-1 tropism by which certain individuals are not readily infected by the virus. In the body two chemokine receptors, CCR5 and CXCR4, are known as the coreceptors for effective HIV entry (*16*). Macrophage-tropic (M-tropic) strains of HIV primarily utilize CCR5 as their coreceptor for entry into cells (*17*−*21*), whereas T cell line-tropic (TCL-tropic) strains are selective for CXCR4 (*22*). The specific chemokines that have been shown to interact with CCR5 are MIP-1α (CCL3), MIP-1β (CCL4), MCP-2 (CCL8), and RANTES (CCL5). All of these chemokines have been shown to inhibit HIV-1 entry into cells (*23*−*25*). In addition, small-molecule CCR5 antagonists such as vicriviroc (SCH-D; Schering-Plough) and maraviroc (UK-427,857; Pfizer) have been shown to significantly reduce viral load in HIV-1 patients, demonstrating the therapeutic utility of targeting CCR5 as a means to treat HIV-1/AIDS patients (*26*).

Originally isolated from the hemofiltrate of chronic renal failure patients, plasmatic hemofiltrate CC chemokine 1 or CC chemokine ligand 14 (CCL14) is a prototypical CC-type chemokine. CCL14 is found in human plasma at high concentrations (1.5−10 nM) and is constitutively expressed in many different tissues (*27*). CCL14 utilizes CCR1, CCR3, and CCR5 for chemotaxis and is involved in the activation of eosinophils, monocytes, and T lymphoblasts. The full-length CCL14 of 74 amino acids is naturally turned into a high-affinity ligand for CCR5 through proteolytic processing by urokinase plasminogen activator and plasmin (*28*). This cleaved form, CCL14 [9−74], has been shown to block HIV entry and replication (*29*, *30*), whereas the CCL14 itself has not. Likewise, the CCL14 [9−74] is able to signal by inducing Ca^{2+} flux and migration of different leukocytes (*29*), whereas CCL14 is not, consistent with the difference in their CCR5 binding affinity.

In our study, we report the high-resolution crystal structures of CCL14 and CCL14 [9−74]. Combined with data from analytical ultracentrifuge and BIAcore studies, we demonstrate that CCL14 [9−74] can convert to a monomer more readily than CCL14 at physiological concentrations. In vitro assays confirm that CCL14 [9−74], not CCL14, is able to induce calcium flux and to inhibit HIV entry at a concentration where CCL14 [9−74] is a monomer and CCL14 is a dimer.

MATERIALS AND METHODS

Crystallization and Data Collection. Crystals of CCL14 were grown at room temperature by hanging drop vapor diffusion. Each drop contained equal volumes of protein solution and reservoir solution. CCL14 crystals were grown by mixing equal volumes (2 μL each) of protein (20 mg/mL, in 0.2 M NaCl and 10 mM MES, pH 6.0) and reservoir solution. CCL14 crystals grew overnight in solution no. 21 from the Hampton PEG/ion screen containing 0.2 M sodium formate and 20% (w/v) polyethylene glycol 3350 (PEG 3350). CCL14 [9−74] crystals were grown by mixing equal volumes (2 μL each) of protein (14 mg/mL, in 0.25 M NaCl and 20 mM MES, pH 6.2) and reservoir solution. CCL14 [9−74] crystals grew after 2 days in solution no. 18 from the Hampton screen 1 containing 0.2 M magnesium acetate tetrahydrate, 0.1 M sodium cacodylate trihydrate, pH 6.5, and 20% PEG 8000. For X-ray diffraction experiments, crystals were taken directly from the droplets with a fiber loop and flash frozen in liquid N_2 with no cryoprotectant. The diffraction data for CCL14 were collected at beamline 9.1 at the Stanford Synchrotron Radiation Laboratory, and the CCL14 [9−74] diffraction data were collected at the Advanced Light Source on beamline 8.2.1. X-ray data sets were integrated and scaled using the program HKL-2000 version 0.98.692i (*31*). The space group of CCL14 was found to be *C*2 with unit cell dimensions $a = 94.35$ Å, $b = 78.07$ Å, $c = 59.64$ Å, $\alpha = 90°$, $\beta = 121.65°$, and $\gamma = 90°$. The space group of CCL14 [9−74] was found to be $P2_12_12_1$ with unit cell dimensions $a = 56.14$ Å, $b = 57.55$ Å, $c = 85.44$ Å, and $\alpha = \beta = \gamma = 90°$.

Crystal Structure Determination and Refinement. The crystal structures of CCL14 and CCL14 [9−74] were solved by molecular replacement with the program Phaser (*32*−*34*) in the CCP4 program suite (*35*). The search model for CCL14 was the AOP RANTES dimer (PDB code 1B3A) (*36*). A rotation and translation search using the dimer of AOP RANTES identified two dimers in the asymmetric unit, which by 2-fold crystallographic symmetry form an octameric packing assembly. The molecular replacement search for CCL14 [9−74] had a solution for two dimers in the asymmetric unit, which did not generate the same octameric assembly of full-length CCL14. The protein chain models were built using the programs ARP/wARP version 6.1 (*37*, *38*), O (*39*), and Coot version 0.2 (*40*, *41*). The program Refmac5 version (*35*, *42*) was used to refine both structures.

The final crystallographic *R* factor and free *R* factor for CCL14 are 18.7% and 23.4%, respectively, for reflections within 56−2.2 Å. Moreover, the final crystallographic *R* factor and free *R* factor for CCL14 [9−74] are 17.4% and 22.8%, respectively, for reflections within 46.9−1.8 Å. The root mean square deviations in bond lengths and bond angles for CCL14 are 0.021 and 1.69 Å, respectively. The root mean square deviations in bond lengths and bond angles for CCL14 [9−74] are 0.013 and 1.24 Å, respectively. The Ramachan-

dran plot calculated for the final CCL14 model using the program PROCHECK (*43*) shows that the conformations of 96.9% of the residues are located within the most favored regions and 3.1% of the residues are located within the additionally allowed regions. The Ramachandran plot calculated for the final CCL14 [9−74] model shows that the conformations of 95.9% of the residues are located within the most favored regions and 4.1% of residues are located within the additionally allowed regions. All water molecules have densities of 1σ or greater in the final $2F_o - F_c$ map.

Sedimentation Equilibrium Ultracentrifugation. All protein samples were dialyzed in 10 mM Na_2PO_4 and 150 mM NaCl at pH 7.5. Sedimentation equilibrium analytical ultracentrifugation experiments were performed using a Beckman Optima XL-I analytical ultracentrifuge (Beckman, CA) at 20 °C and six-channel centerpieces. Three pairs of blanks and protein samples at three different concentrations were loaded at a volume of 120 μL each and were centrifuged against 130 μL of the equivalent buffer blank. Centrifugation was performed at rotor speeds and durations of 20000 rpm for 19 h, 27500 rpm for 18 h, 35000 rpm for 17 h, 42500 rpm for 15 h, and 50000 rpm for 13 h. At each speed the cells were scanned across their radius at 280 or 220 nm. To confirm equilibrium, a second scan was taken 1 h later and compared to the first scan. Since low concentrations are required to measure an accurate K_d, absorbances were measured at 220 nm for all samples. The protein loading concentrations used were 2.4, 3.2, and 6.4 μM for all samples.

Analysis was performed by a global nonlinear least-squares method using the program UltraScan version 9.1 (*44*). For CCL14 and CCL14 E15A, data were fitted to a one-component ideal model, and for CCL14 [9−74] and CCL14 [9−74] E15A, the data were fitted to a monomer−dimer−tetramer equilibrium model; 95% confidence intervals were estimated by Monte Carlo analysis. CCL14 E15A and CCL14 [9−74] E15A are single-point mutants replacing Glu^{15} to Ala. The mutation was predicted to disrupt the tetrameric assembly interface where Glu^{15} is found. The molecular masses that were calculated from the fit indicated the oligomeric state of the protein under the specific solution condition. The density was calculated on the basis of the composition of the buffer used, via the buffer calculation module within UltraScan (*44*). The partial specific volume ($\bar{v}$) was calculated on the basis of its primary amino acid sequence and the temperature (20 °C).

Surface Plasmon Resonance Analysis (BIAcore). CCL14, CCL14 [9−74], CCL14 E15A, and CCL14 [9−74] E15A binding analyses were performed on a BIAcore 1000 instrument (BIAcore). Primary amine coupling was used to immobilize CCL14 on a CM4 and CM5 sensor chip (BIAcore) in flow cell 2 and to immobilize CCL14 [9−74] (BIAcore) in flow cell 3. Flow cell 1 was used as a reference surface. The chemokines were immobilized at a concentration of 5 μg/mL in filtered 10 mM sodium acetate buffer at pH 5.0. The proteins were immobilized by pulsing the injection of chemokine over the chip surface at a flow rate of 10 μL/min until the desired number of response units (500 RU) was reached. The binding assays were performed in filtered 10 mM HEPES, pH 7.5, 150 mM NaCl, 3 mM EDTA, and 0.005% Tween 20 at a flow rate of 30 μL/min for a total of 2 min. Seven different concentrations, including a zero concentration, of each chemokine were run. Global fits to binding curves using a 1:1 binding with the mass transfer model and separate fits of the association (k_{on}) and dissociation (k_{off}) rate constants were used, both yielding similar results. The overall K_d was then calculated using the BIAEVALUATION version 4.1 software (BIAcore).

Table 1: Data Collection and Model Refinement Statistics

	CCL14	CCL14 [9−74]
space group	*C*2	$P2_12_12_1$
unit cell parameters		
a (Å)	94.3	56.1
b (Å)	78.1	57.6
c (Å)	59.6	85.4
β (deg)	121.7	90.0
data collection statistics		
beamline	9.1 SSRL	8.2.1 ALS
wavelength (Å)	1.000	1.000
resolution range (Å)	50−2.23 (2.31−2.23)	50−1.82 (1.89−1.82)
observed reflections	74369	203161
unique reflections	17814	25453
redundancy	4.2 (4.2)[b]	8.0 (7.3)[b]
R_{merge} (%)	3.9 (10.0)[b]	5.4 (17.0)[b]
mean $I/\sigma(I)$	30.98 (14.3)[b]	35.32 (11.2)[b]
completeness (%)	98.9 (99.2)[b]	99.6 (96.3)[b]
refinement statistics		
R_{cryst} (%)	18.7	17.35
R_{free} (%)[a]	23.4	22.786
average *B* factor (Å^2)	37.739	14.096
root mean square deviation		
bond lengths (Å)	0.021	0.013
bond angles (Å)	1.685	1.243
no. of atoms, total	2314	2467
protein	2130	2102
water	184	365
no. of missing residues	40	9
Ramachandran plot (%)		
most favored	96.9	95.9
additional allowed	3.1	4.1
generously allowed	0.0	0.0

[a] Calculated from 5% of data not used in refinement. [b] Numbers in parentheses correspond to highest resolution shell (Å).

Calcium Flux Assay. CCR5 transfected 293 T were detached from a T-75 cell culture flask using cell dissociation buffer, and after washing two times with HBSS buffer, cells were resuspended at 2.5×10^6 cells/mL. The cells were then labeled with Fluo-4AM (Molecular Probes no. P-3000MP) at a final concentration of 4 μg/mL for 60 min at room temperature in the dark. The labeled cells were washed twice in HBSS buffer and resuspended at 2.5×10^6 cells/mL. Then 150 μL of the labeled cell suspension was transferred to a poly(D-lysine)-coated 96-well plate (Biocoat no. 359109) and centrifuged at 500 rpm for 1 min. Various concentrations (50 μL) of CCL14 and CCL14 mutants were added, and the increase in intracellular calcium was determined using FLIPR.

HIV Infectivity Assay. PBMCs were isolated from buffy coats from HIV-seronegative donors. Cells were stimulated with anti-CD3 antibody and IL-2 for 48 h followed by depletion of CD8+ T cells. Then, 150000 cells were seeded per well in 96-well flat-bottom plates. Cells were preincubated with CCL14 protein in triplicate at a range of concentrations up to 1600 nM. After 2 h preincubation, cells were infected with luciferase HIV pseudotyped with the CCR5 tropic JRFL envelope protein that is capable of a single round of viral entry and infection (*45*). Following

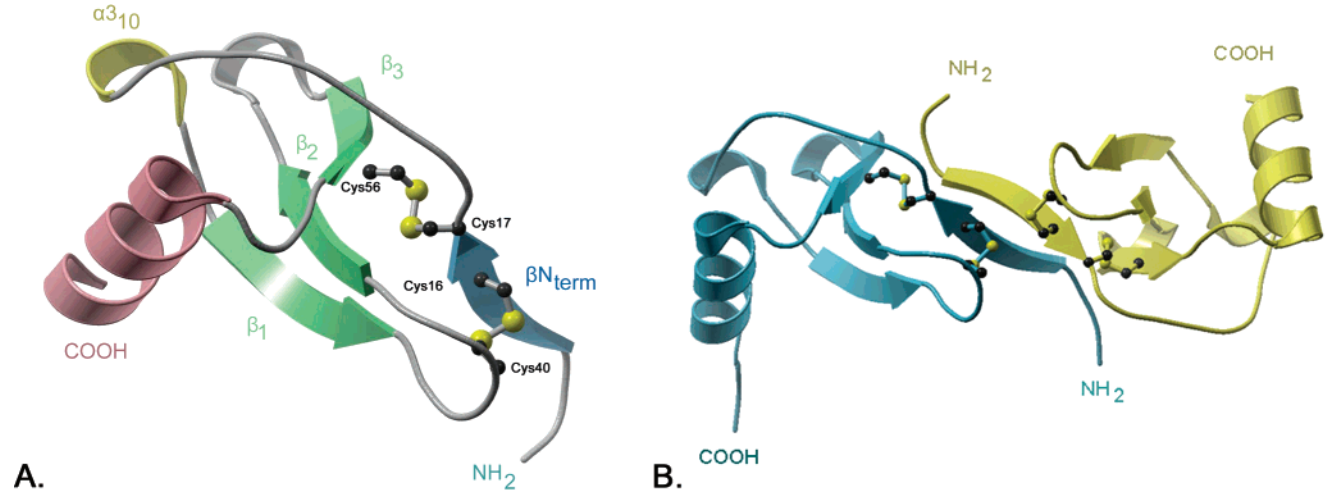

FIGURE 1: Secondary structure of the CCL14 monomer and dimer. (A) The CCL14 monomer shows similarities to the conserved CC-type chemokine fold characterized by three antiparallel β-sheets followed by a C-terminal α-helix, where β-strands are illustrated in blue and green, helices are shown in yellow and pink, and cysteines which form the two disulfide bonds are shown in yellow. (B) The dimer interface is composed of amino acid contacts between the NH_2-terminal strands βN_{term} of each monomer. Two disulfide bonds formed by the four highly conserved cysteine residues, which help to stabilize the overall structure, are oriented in a similar fashion between CCL14 and CCL5. As seen here the three-stranded antiparallel β-sheet and COOH-terminal α-helix are the core structural scaffold of the CC chemokine family. Individual monomers are presented in blue and yellow. Figures were prepared and rendered using MOLSCRIPT version 2.1.2 (*63*) and POV-Ray (*64*).

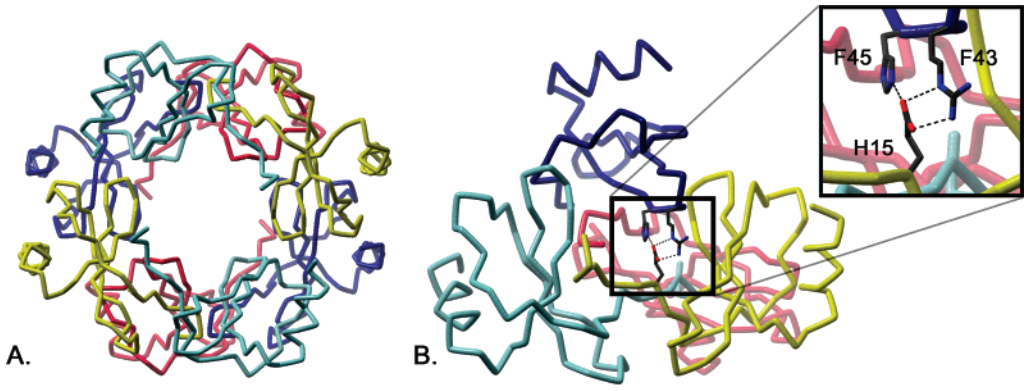

FIGURE 2: CCL14 and CCL14 [9−74] crystal structures. (A) The CCL14 crystal structure is illustrated where each color represents monomers A, B, C, and D in the asymmetric unit. The asymmetric unit consists of a tetramer which is built by two dimers such that dimer 1 is composed of the monomers A−B (red−blue) and dimer 2 is composed of monomers C−D (yellow−teal). By a 2-fold symmetry operation, the two tetramers form an octameric assembly. (B) The CCL14 [9−74] crystal structure is illustrated where each color represents monomers E, F, G, and H in the asymmetric unit. This tetrameric assembly differs from that of the CCL14 structure shown in (A). There can be no octamer assembly that can be formed by any symmetry mates of CCL14 [9−74] in the crystal. Two dimers are shown, where dimer 1 is composed of monomers E−H (teal−yellow) and dimer 2 is composed of monomers F−G (blue−red). The figure on the right of the tetramer zooms into the core of the tetrameric assembly where residue Glu15 resides. The numbers in the zoomed-in window represent the monomer (F or H) followed by the residue number. Figures were prepared and rendered using MOLSCRIPT version 2.1.2 (*63*) and POV-Ray (*64*).

48 h of incubation, cells were lysed and assayed for luciferase activity in a luminometer. The percent entry is calculated for each dose tested by the following formula: [(level of luciferase activity observed in the absence of CCL14 protein)/(level of luciferase observed in the presence of CCL14 protein)] × 100. The level of inhibition is plotted against concentration, and an IC_{50} (amount of protein required to block 50% entry) and IC_{90} (amount of protein required to block 90% entry) are calculated.

RESULTS

Structures of CCL14 and CCL14 [9−74]. The structures of CCL14 and CCL14 [9−74] have been solved by molecular replacement using the program Phaser (*32*−*34*) at a resolution of 2.2 Å for CCL14 in space group *C*2 and 1.8 Å for CCL14 [9−74] in space group $P2_12_12_1$ (Table 1). The monomeric subunits of these structures are characterized by the general CC chemokine fold, consisting of a three-stranded antiparallel β-sheet in a Greek key motif, connected by loops and followed by a C-terminal α-helix (Figure 1A). These structures also contain some common chemokine features such as an NH_2-terminal β-strand (βN_{term}), from Ser^{14} to Cys^{17}, followed by a short $\alpha 3_{10}$ helix, from Arg^{27} to Arg^{29}, which directly precedes the first β-strand of the three-stranded antiparallel β-sheet. The three β-strands that create the antiparallel β-sheet are comprised of residues Ile^{30}−Glu^{35} (β1), Ile^{45}−Thr^{49} (β2), and Gly^{52}−Thr^{57} (β3). The C-terminal α-helix is formed by residues Lys^{62}−Met^{71} (Figure 1A). Two disulfide bridges are formed between the following four cysteine residues: Cys^{16}−Cys^{40} and Cys^{17}−Cys^{56}. These two disulfide bridges link the NH_2-terminal region with β3 and with the hairpin loop between β1 and β2, stabilizing the

monomeric structure. Interactions between two antiparallel β-strands ($\beta N_{term}-\beta N_{term}$) stabilize the dimer without a covalent bond between them (Figure 1B). The two homodimers (A−B and C−D of CCL14 or E−H and F−G of CCL14 [9−74]) assume the same intermolecular interaction resulting in the same dimeric configuration. At this high resolution it is very clear that the first nine amino acids on the NH_2 terminus are not present in the electron density of any monomers in the CCL14 structure, indicating high mobility in this region.

Crystal Structures Reveal Higher Order Oligomers for CCL14 and CCL14 [9−74]. Although both CCL14 and CCL14 [9−74] are similar in monomeric and dimeric structures, they differ slightly among those found in the asymmetric unit. CCL14 forms a tetramer in the asymmetric unit and by 2-fold symmetry creates an octamer. In all four monomers (A, B, C, and D) in CCL14, the first nine residues, Thr^1-Gly^9, were not present in the electron density maps. $Lys^{72}-Asn^{74}$ in monomer A and Asn^{74} in monomer D are also disordered (Figure 2A). CCL14 [9−74] also packs as a tetramer (monomers E, F, G, and H) in the asymmetric unit, but in contrast to the octameric quaternary state of CCL14, it does not form a higher order oligomer with any symmetry mates. In monomers F, G, and H of CCL14 [9−74], the COOH-terminal residues $Lys^{72}-Asn^{74}$ are disordered (Figure 2B).

To test if the difference in quaternary structure plays a role in the activity of the chemokine, we designed two point mutants: CCL14 E15A and CCL14 [9−74] E15A. The CCL14 [9−74] E15A mutation was designed to destabilize the tetramer assembly by placing a point mutation in the dimer interface at residue Glu^{15} (Figure 2), and CCL14 E15A was created as a control. Interestingly, the point mutation did alter the tetrameric arrangement of CCL14 [9−74] to that of CCL14 forming the octameric packing, and as illustrated below, CCL14 E15A remained inactive, but CCL14 [9−74] E15A increased HIV inhibition by 10- and 50-fold (IC_{50} and IC_{90}) compared to that of the wild type.

Concentration-Dependent Inhibition of HIV-1 Entry and Ca^{2+} Flux Activity. The ability of the CCL14 proteins to inhibit entry of HIV-1 was performed by testing their efficacy to block entry of a CCR5 tropic recombinant HIV-1 virus containing the luciferase reporter gene into activated CD4 T-cells. While both CCL14 [9−74] and CCL14 [9−74] E15A mediated greater than 95% inhibition of HIV-1 entry, neither CCL14 nor CCL14 E15A demonstrated any dose-dependent inhibition of HIV-1 entry as shown for a representative donor in Figure 3A. The IC_{50} and IC_{90} concentrations for CCL14 [9−74] were 146 nM and 6.3 μM, respectively, while for CCL14 [9−74] E15A they were 14.2 and 260 nM. Hence introduction of the E15A mutation reduces the IC_{50} and IC_{90} concentrations by 10- and 50-fold.

Ca^{2+} flux assays were completed in parallel to test the ability to signal through CCR5 by inducing an increase in intracellular Ca^{2+} concentrations. Correlating with the data from the HIV-1 infectivity assay, the truncated CCL14 [9−74] and CCL14 [9−74] E15A were able to induce high levels of intracellular Ca^{2+}, demonstrating their ability to bind to CCR5 and signal. In contrast, mobilization of intracellular Ca^{2+} was not detected by CCL14 and CCL14 E15A (Figure 3B). We also note that there is an insignificant difference between CCL14 [9−74] and CCL14 [9−74] E15A in the calcium flux assay. Although this contrasts to the CCL14 [9−74] E15A data showing an increased inhibition of HIV-infectivity, as reflected in the ~10-fold reduction of the IC-50 concentration compared to CCL14 [9−74], alteration of the tetrameric assembly of CCL14 [9−74] by the introduction of the E15A mutation is an observation potentially useful in developing anti-HIV therapeutics.

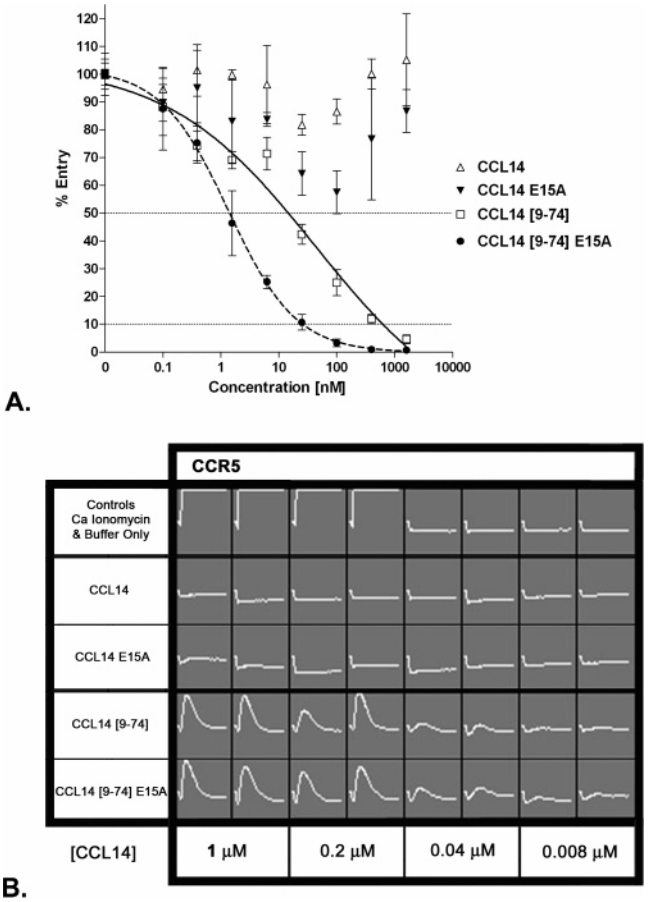

FIGURE 3: HIV entry inhibition and calcium mobilization by CCL14 proteins. (A) Inhibition of CCR5-tropic HIV-1 virus infection of activated human PBMCs by CCL14 proteins was determined. CCL14 [9−74] and CCL14 [9−74] E15A blocked greater than 90% of HIV infection while full-length CCL14 proteins had no dose-dependent effect. CCL14 [9−74] demonstrated an IC_{50} of 146 nM and an IC_{90} of 6.3 uM while CCL14 E15A [9−74] demonstrates IC_{50} and IC_{90} of 14.2 and 260 nM. (B) Intracellular Ca^{2+} levels were measured in the presence of CCL14 and mutants at four different chemokine concentrations (bottom row). Ca ionomycin and buffer only were used as positive and negative controls, respectively. Ca ionomycin controls are illustrated in the left four boxes in the first row, and the buffer only control is shown in the right four boxes in the first row. Full-length CCL14 and CCL14 E15A do not produce an increase in intracellular Ca^{2+} levels (top two rows under controls). Truncated CCL14 [9−74] and CCL14 [9−74] E15A show an increase in intracellular Ca^{2+} levels at concentrations from 0.2 to 1 μM (bottom two rows). Their effective concentrations are approximately similar to each other.

Monomer Dissociation Rates Determined by Analytical Ultracentrifugation. Crystal structures of CCL14 and CCL14 [9−74] dimers do not show conformational difference between the two to account for the difference in functional binding. Since CCL14 is found in human plasma at a concentration around 10 nM (*27*), sedimentation equilibrium absorbance analytical ultracentrifugation experiments were used to measure the oligomeric state at low concentrations.

Table 2: Equilibrium Sedimentation Analytical Ultracentrifugation Analysis of CCL14 and CCL14 [9−74]

sample	MW (Da)	$K_{d1,2}$ (μM)	$K_{d1,4}$ (M^3)	best fit model
CCL14	1.628×10^4 (+85/−67)[a]			ideal one component
CCL14 E15A	1.677×10^4 (+68/−71)[a]			ideal one component
CCL14 [9−74]	8284 (+665/−496)[a]	12.32 (+52.34/−9.33)[a]	12.35×10^{-17} ($+9.94 \times 10^{-17}$/-6.56×10^{-17})[a] ($EC_{1,4} = 4.98$ μM)[b]	monomer−dimer−tetramer
CCL14 [9−74] E15A	8336 (+879/−1036)[a]	10.00 (+14.60/−3.90)[a]	1.319×10^{-17} ($+1.25 \times 10^{-17}$/-0.678×10^{-17})[a] ($EC_{1,4} = 2.36$ μM)[b]	monomer−dimer−tetramer

[a] The numbers in parentheses represent the 95% confidence intervals for the determined parameters. [b] EC represents the equilibrium concentration.

By measuring absorbance at 220 nm in 10 mM phosphate buffer, CCL14 and CCL14 E15A remain homogeneously as a dimer in solution at a concentration as low as 100 nM, indicating that the K_d for the monomer−dimer equilibrium must be far less than 100 nM. This analysis is insufficient to show if they will form monomeric states (Table 2), when diluted to in vivo concentration. However, data for CCL14 [9−74] and CCL14 [9−74] E15A were fit very well to a monomer−dimer−tetramer model using the program UltraScan (*44*), and the equilibrium concentration (EC) of the dissociation of tetramers to monomers was found to be in the low micromolar concentrations, with $EC_{1,4}$'s of 4.98 and 2.36 μM for CCL14 [9−74] and CCL14 [9−74] E15A, respectively (Table 2, Figure 4).

Since absorbance-based analytical ultracentrifugation is not suitable to derive the monomer−dimer equilibrium constants smaller than 100 nM for full-length CCL14 (Table 2), surface plasmon resonance (BIAcore) analysis was performed as an alternative method to estimate the binding affinities of the chemokines CCL14 and CCL14 [9−74]. We assumed that, at very low concentration, the noncovalent CCL14 dimers must dissociate into monomers. In these experiments, each chemokine was immobilized at a low concentration where it was extensively diluted to a monomeric state on the BIAcore chip surface. A blank surface in flow cell 1 was used as a control. At these low concentrations, therefore, protein binding of CCL14 and CCL14 [9−74] in the eluent can simulate dimerization as measured as their ability to bind to their corresponding immobilized partner. The equilibrium dissociation constants, K_d's, for CCL14 and CCL14 [9−74] are 9.84 and 667 nM, respectively, and the K_d's for CCL14 E15A and CCL14 [9−74] E15A are 15.3 and 664 nM, respectively. These results show that the dimerization stability of CCL14 is about 60-fold higher than that of CCL14 [9−74], and CCL14 E15A is about 40-fold higher than that of CCL14 [9−74] E15A.

DISCUSSION

Proteolytic processing of the first eight amino acids activates CCL14 prior to its binding to CCR5 (*29*, *30*, *46*). X-ray crystallographic analysis shows that CCL14 and CCL14 [9−74] do not have conformational differences in their monomeric fold and dimeric assemblies, thus also revealing similarities to other CC chemokine structures such as CCL5 (*47*, *48*), CCL4 (*49*), and CCL2 (*50*). A study on NH_2-terminal processing through the creation of CCL14 variants with lengths ranging from CCL14 [6−74] to CCL14 [12−74] has shown that only CCL14 [9−74] and CCL14 [10−74] block HIV infectivity (*30*). Furthermore, it is well-known that certain residues in the NH_2-terminal region of many other CC chemokines are involved in controlling receptor binding and activation (*11*, *51*−*55*). Many have also revealed that NH_2-terminal modifications to chemokines can result in antagonistic, agonistic, or superagonistic properties. A recent study on the NH_2-terminally modified CCL14 analogue, *n*-nonanoyl-CC chemokine ligand 14, shows the induction of the internalization of CCR3 and desensitization of CCR3-mediated calcium release (*56*). The amino acids directly adjacent to the first eight residues in CCL14 may also be important for identification by the receptor such that the first eight amino acids need to be removed in order for binding and correct recognition to occur. However, in light of our structural analysis it is unclear how the flexibility of the first eight or nine amino acids may be an important property that affects the ability of CCL14 to bind to CCR5.

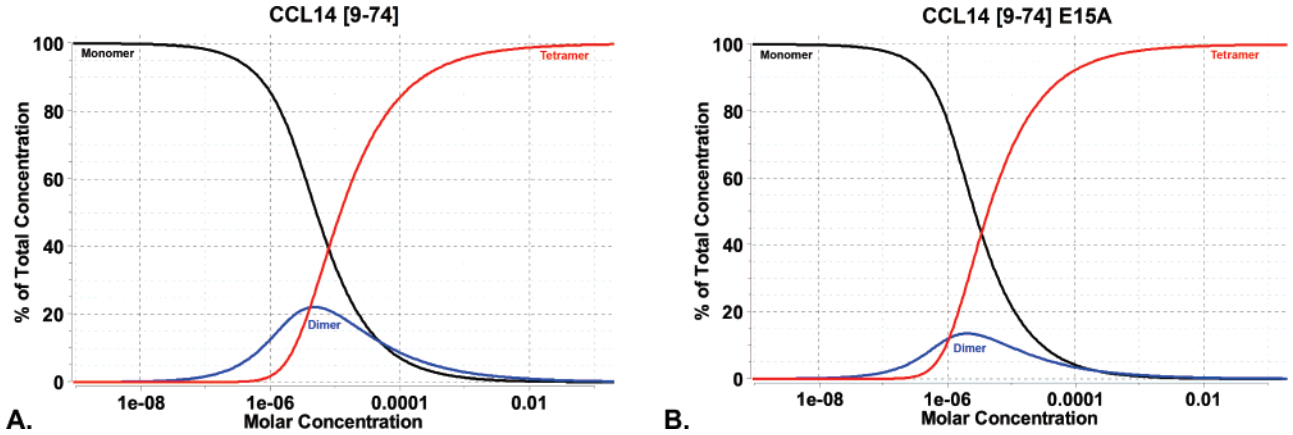

FIGURE 4: Self-association profiles for CCL14 [9−74] and CCL14 [9−74] E15A. Self-association curve-fit profiles were generated for (A) CCL14 [9−74] and (B) CCL14 [9−74] E15A from the analytical ultracentrifuge data using the program UltraScan (*44*). See Materials and Methods for analytical details. The lines represent the different oligomeric states present in the samples as follows: black (monomer), blue (dimer), and red (tetramer).

Here we suggest that CCL14's ability to monomerize affects its activity. Using analytical ultracentrifugation studies, performed at low concentrations which were closer to those found in vivo, the dissociation of dimers to monomers of CCL14 [9−74] happens at near-physiological concentration. If we assume that the monomerization of CCL14 is a step in activation, it is unclear how the flexible NH_2-terminal eight residues contribute to the stability of the dimer. The possibility that the monomer is the active form of chemokines was first proposed when the functional unit of a chemically synthesized analogue of the CXC, chemokine IL-8, was shown to be a monomer (*57*). Since then many studies have been carried out on different CC chemokines including CCL1 (*58*), CCL2 (*51*, *58*), CCL3 (*59*, *60*), CCL4 (*52*, *53*), CCL7 (*61*), and CCL8 (*61*), all suggesting that the monomer is important for binding and activation of chemokine receptors. Some analogues of other CC chemokines obtained by modification to their NH_2 terminus still bind to their receptors but do not signal and thus act as antagonists. Therefore, additional mechanisms of activation caused by NH_2-terminal alterations may also play a role (*62*).

The chemokine activity assays, analytical ultracentrifugation data, and BIAcore data presented here show that inactive CCL14 forms an approximately 60-fold more stable dimer than that of active CCL14 [9−74]. Together, these results suggest how the CCL14 dimer may result in the active CCL14 [9−74] monomer at physiological concentration. Although CCL14 is found circulating in the blood at 10 nM (*27*), it is well-known that chemokines form gradients when they home to sites of infection. With this in mind, CCL14 is probably at concentrations that are higher than 10 nM at the time of activation and are near the concentration where CCL14 is dimeric and CCL14 [9−74] is monomeric and thus may account for their difference in activity.

ACKNOWLEDGMENT

We thank Andy Garcia, Jingli Cong, Erin Stracuzzi, Jason Bock, and Kimberly Florence for help with protein production and bioassay.

REFERENCES

1. Murphy, P. M., Baggiolini, M., Charo, I. F., Hebert, C. A., Horuk, R., Matsushima, K., Miller, L. H., Oppenheim, J. J., and Power, C. A. (2000) International Union of Pharmacology. XXII. Nomenclature for chemokine receptors, *Pharmacol Rev. 52*, 145−176.
2. Murphy, P. M. (1996) Chemokine receptors: structure, function and role in microbial pathogenesis, *Cytokine Growth Factor Rev. 7*, 47−64.
3. Moser, B., Wolf, M., Walz, A., and Loetscher, P. (2004) Chemokines: multiple levels of leukocyte migration control, *Trends Immunol. 25*, 75−84.
4. Baggiolini, M., Dewald, B., and Moser, B. (1997) Human chemokines: an update, *Annu. Rev. Immunol. 15*, 675−705.
5. Proudfoot, A. E. (1998) The chemokine family. Potential therapeutic targets from allergy to HIV infection, *Eur. J. Dermatol. 8*, 147−157.
6. Bacon, K., Baggiolini, M., Broxmeyer, H., Horuk, R., Lindley, I., Mantovani, A., Maysushima, K., Murphy, P., Nomiyama, H., Oppenheim, J., Rot, A., Schall, T., Tsang, M., Thorpe, R., Van Damme, J., Wadhwa, M., Yoshie, O., Zlotnik, A., and Zoon, K. (2003) Chemokine/chemokine receptor nomenclature, *Cytokine 21*, 48−49.
7. St. Charles, R., Walz, D. A., and Edwards, B. F. (1989) The three-dimensional structure of bovine platelet factor 4 at 3.0-Å resolution, *J. Biol. Chem. 264*, 2092−2099.
8. Clore, G. M., Appella, E., Yamada, M., Matsushima, K., and Gronenborn, A. M. (1990) Three-dimensional structure of interleukin 8 in solution, *Biochemistry 29*, 1689−1696.
9. Baldwin, E. T., Weber, I. T., St. Charles, R., Xuan, J. C., Appella, E., Yamada, M., Matsushima, K., Edwards, B. F., Clore, G. M., Gronenborn, A. M., et al. (1991) Crystal structure of interleukin 8: symbiosis of NMR and crystallography, *Proc. Natl. Acad. Sci. U.S.A. 88*, 502−506.
10. Clore, G. M., and Gronenborn, A. M. (1995) Three-dimensional structures of alpha and beta chemokines, *FASEB J. 9*, 57−62.
11. Clark-Lewis, I., Kim, K. S., Rajarathnam, K., Gong, J. H., Dewald, B., Moser, B., Baggiolini, M., and Sykes, B. D. (1995) Structure-activity relationships of chemokines, *J. Leukocyte Biol. 57*, 703−711.
12. Smit, J. J., and Lukacs, N. W. (2006) A closer look at chemokines and their role in asthmatic responses, *Eur. J. Pharmacol. 533*, 277−288.
13. Nelken, N. A., Coughlin, S. R., Gordon, D., and Wilcox, J. N. (1991) Monocyte chemoattractant protein-1 in human atheromatous plaques, *J. Clin. Invest. 88*, 1121−1127.
14. Koch, A. E., Kunkel, S. L., Harlow, L. A., Mazarakis, D. D., Haines, G. K., Burdick, M. D., Pope, R. M., Walz, A., and Strieter, R. M. (1994) Epithelial neutrophil activating peptide-78: a novel chemotactic cytokine for neutrophils in arthritis, *J. Clin. Invest. 94*, 1012−1018.
15. Robinson, E., Keystone, E. C., Schall, T. J., Gillett, N., and Fish, E. N. (1995) Chemokine expression in rheumatoid arthritis (RA): evidence of RANTES and macrophage inflammatory protein (MIP)-1 beta production by synovial T cells, *Clin. Exp. Immunol. 101*, 398−407.
16. Berger, E. A., Murphy, P. M., and Farber, J. M. (1999) Chemokine receptors as HIV-1 coreceptors: roles in viral entry, tropism, and disease, *Annu. Rev. Immunol. 17*, 657−700.
17. Alkhatib, G., Combadiere, C., Broder, C. C., Feng, Y., Kennedy, P. E., Murphy, P. M., and Berger, E. A. (1996) CC CKR5: a RANTES, MIP-1alpha, MIP-1beta receptor as a fusion cofactor for macrophage-tropic HIV-1, *Science 272*, 1955−1958.
18. Doranz, B. J., Rucker, J., Yi, Y., Smyth, R. J., Samson, M., Peiper, S. C., Parmentier, M., Collman, R. G., and Doms, R. W. (1996) A dual-tropic primary HIV-1 isolate that uses fusin and the beta-chemokine receptors CKR-5, CKR-3, and CKR-2b as fusion cofactors, *Cell 85*, 1149−1158.
19. Dragic, T., Litwin, V., Allaway, G. P., Martin, S. R., Huang, Y., Nagashima, K. A., Cayanan, C., Maddon, P. J., Koup, R. A., Moore, J. P., and Paxton, W. A. (1996) HIV-1 entry into CD4+ cells is mediated by the chemokine receptor CC-CKR-5, *Nature 381*, 667−673.
20. Choe, H., Farzan, M., Sun, Y., Sullivan, N., Rollins, B., Ponath, P. D., Wu, L., Mackay, C. R., LaRosa, G., Newman, W., Gerard, N., Gerard, C., and Sodroski, J. (1996) The beta-chemokine receptors CCR3 and CCR5 facilitate infection by primary HIV-1 isolates, *Cell 85*, 1135−1148.
21. Deng, H., Liu, R., Ellmeier, W., Choe, S., Unutmaz, D., Burkhart, M., Di Marzio, P., Marmon, S., Sutton, R. E., Hill, C. M., Davis, C. B., Peiper, S. C., Schall, T. J., Littman, D. R., and Landau, N. R. (1996) Identification of a major co-receptor for primary isolates of HIV-1, *Nature 381*, 661−666.
22. Feng, Y., Broder, C. C., Kennedy, P. E., and Berger, E. A. (1996) HIV-1 entry cofactor: functional cDNA cloning of a seven-transmembrane, G protein-coupled receptor, *Science 272*, 872−877.
23. Gong, W., Howard, O. M., Turpin, J. A., Grimm, M. C., Ueda, H., Gray, P. W., Raport, C. J., Oppenheim, J. J., and Wang, J. M. (1998) Monocyte chemotactic protein-2 activates CCR5 and blocks CD4/CCR5-mediated HIV-1 entry/replication, *J. Biol. Chem. 273*, 4289−4292.
24. Cocchi, F., DeVico, A. L., Garzino-Demo, A., Arya, S. K., Gallo, R. C., and Lusso, P. (1995) Identification of RANTES, MIP-1 alpha, and MIP-1 beta as the major HIV-suppressive factors produced by CD8+ T cells, *Science 270*, 1811−1815.
25. Greco, G., Mackewicz, C., and Levy, J. A. (1999) Sensitivity of human immunodeficiency virus infection to various alpha, beta and gamma chemokines, *J. Gen. Virol. 80* (Part 9), 2369−2373.
26. Westby, M., and van der Ryst, E. (2005) CCR5 antagonists: host-targeted antivirals for the treatment of HIV infection, *Antiviral Chem. Chemother. 16*, 339−354.
27. Schulz-Knappe, P., Magert, H. J., Dewald, B., Meyer, M., Cetin, Y., Kubbies, M., Tomeczkowski, J., Kirchhoff, K., Raida, M., Adermann, K., Kist, A., Reinecke, M., Sillard, R., Pardigol, A.,

Uguccioni, M., Baggiolini, M., and Forssmann, W. G. (1996) HCC-1, a novel chemokine from human plasma, *J. Exp. Med. 183*, 295−299.
28. Vakili, J., Standker, L., Detheux, M., Vassart, G., Forssmann, W. G., and Parmentier, M. (2001) Urokinase plasminogen activator and plasmin efficiently convert hemofiltrate CC chemokine 1 into its active, *J. Immunol. 167*, 3406−3413.
29. Detheux, M., Standker, L., Vakili, J., Munch, J., Forssmann, U., Adermann, K., Pohlmann, S., Vassart, G., Kirchhoff, F., Parmentier, M., and Forssmann, W. G. (2000) Natural proteolytic processing of hemofiltrate CC chemokine 1 generates a potent CC chemokine receptor (CCR)1 and CCR5 agonist with anti-HIV properties, *J. Exp. Med. 192*, 1501−1508.
30. Munch, J., Standker, L., Pohlmann, S., Baribaud, F., Papkalla, A., Rosorius, O., Stauber, R., Sass, G., Heveker, N., Adermann, K., Escher, S., Kluver, E., Doms, R. W., Forssmann, W. G., and Kirchhoff, F. (2002) Hemofiltrate CC chemokine 1[9−74] causes effective internalization of CCR5 and is a potent inhibitor of R5-tropic human immunodeficiency virus type 1 strains in primary T cells and macrophages, *Antimicrob. Agents Chemother. 46*, 982−990.
31. Otwinowski, Z., and Minor, W. (1997) Processing of X-ray diffraction data collected in oscillation mode, *Methods Enzymol. 276*, 307−326.
32. Read, R. J. (2001) Pushing the boundaries of molecular replacement with maximum likelihood, *Acta Crystallogr., Sect. D: Biol. Crystallogr. 57*, 1373−1382.
33. Storoni, L. C., McCoy, A. J., and Read, R. J. (2004) Likelihood-enhanced fast rotation functions, *Acta Crystallogr., Sect. D: Biol. Crystallogr. 60*, 432−438.
34. McCoy, A. J., Grosse-Kunstleve, R. W., Storoni, L. C., and Read, R. J. (2005) Likelihood-enhanced fast translation functions, *Acta Crystallogr., Sect. D: Biol. Crystallogr. 61*, 458−464.
35. Collaborative Computational Project, Number 4 (1994) The CCP4 suite: programs for protein crystallography, *Acta Crystallogr., Sect. D: Biol. Crystallogr. 50*, 760−763.
36. Wilken, J., Hoover, D., Thompson, D. A., Barlow, P. N., McSparron, H., Picard, L., Wlodawer, A., Lubkowski, J., and Kent, S. B. (1999) Total chemical synthesis and high-resolution crystal structure of the potent anti-HIV protein AOP-RANTES, *Chem. Biol. 6*, 43−51.
37. Lamzin, V. S., and Wilson, K. S. (1993) Automated refinement of protein models, *Acta Crystallogr., Sect. D: Biol. Crystallogr. 49*, 129−147.
38. Perrakis, A., Morris, R., and Lamzin, V. S. (1999) Automated protein model building combined with iterative structure refinement, *Nat. Struct. Biol. 6*, 458−463.
39. Jones, T. A., Zou, J. Y., Cowan, S. W., and Kjeldgaard, M. (1991) Improved methods for building protein models in electron density maps and the location of errors in these models, *Acta Crystallogr. A 47* (Part 2), 110−119.
40. Emsley, P., and Cowtan, K. (2004) Coot: model-building tools for molecular graphics, *Acta Crystallogr., Sect. D: Biol. Crystallogr. 60*, 2126−2132.
41. Krissinel, E., and Henrick, K. (2004) Secondary-structure matching (SSM), a new tool for fast protein structure alignment in three dimensions, *Acta Crystallogr., Sect. D: Biol. Crystallogr. 60*, 2256−2268.
42. Murshudov, G. N., Vagin, A. A., and Dodson, E. J. (1997) Refinement of macromolecular structures by the maximum-likelihood method, *Acta Crystallogr., Sect. D: Biol. Crystallogr. 53*, 240−255.
43. Laskowski, R. A., MacArthur, M. W., Moss, D. S., and Thornton, J. M. (1993) PROCHECK: a program to check the stereochemical quality of protein structures, *J. Appl. Crystallogr. 26*, 283−291.
44. Demeler, B. (2005) *UltraScan A Comprehensive Data Analysis Software Package for Analytical Ultracentrifugation Experiments. Modern Analytical Ultracentrifugation: Techniques and Methods* (Scott, D. J., Harding, S. E., and Rowe, A. J., Eds.) pp 210−229, Royal Society of Chemistry, U.K.
45. Moir, S., Lapointe, R., Malaspina, A., Ostrowski, M., Cole, C. E., Chun, T. W., Adelsberger, J., Baseler, M., Hwu, P., and Fauci, A. S. (1999) CD40-mediated induction of CD4 and CXCR4 on B lymphocytes correlates with restricted susceptibility to human immunodeficiency virus type 1 infection: potential role of B lymphocytes as a viral reservoir, *J. Virol. 73*, 7972−7980.
46. Tsou, C. L., Gladue, R. P., Carroll, L. A., Paradis, T., Boyd, J. G., Nelson, R. T., Neote, K., and Charo, I. F. (1998) Identification of C-C chemokine receptor 1 (CCR1) as the monocyte hemofiltrate C-C chemokine (HCC)-1 receptor, *J. Exp. Med. 188*, 603−608.
47. Chung, C. W., Cooke, R. M., Proudfoot, A. E., and Wells, T. N. (1995) The three-dimensional solution structure of RANTES, *Biochemistry 34*, 9307−9314.
48. Skelton, N. J., Aspiras, F., Ogez, J., and Schall, T. J. (1995) Proton NMR assignments and solution conformation of RANTES, a chemokine of the C-C type, *Biochemistry 34*, 5329−5342.
49. Lodi, P. J., Garrett, D. S., Kuszewski, J., Tsang, M. L., Weatherbee, J. A., Leonard, W. J., Gronenborn, A. M., and Clore, G. M. (1994) High-resolution solution structure of the beta chemokine hMIP-1 beta by multidimensional NMR, *Science 263*, 1762−1767.
50. Handel, T. M., and Domaille, P. J. (1996) Heteronuclear (^{1}H, ^{13}C, ^{15}N) NMR assignments and solution structure of the monocyte chemoattractant protein-1 (MCP-1) dimmer, *Biochemistry 35*, 6569−6584.
51. Paavola, C. D., Hemmerich, S., Grunberger, D., Polsky, I., Bloom, A., Freedman, R., Mulkins, M., Bhakta, S., McCarley, D., Wiesent, L., Wong, B., Jarnagin, K., and Handel, T. M. (1998) Monomeric monocyte chemoattractant protein-1 (MCP-1) binds and activates the MCP-1 receptor CCR2B, *J. Biol. Chem. 273*, 33157−33165.
52. Laurence, J. S., Blanpain, C., Burgner, J. W., Parmentier, M., and LiWang, P. J. (2000) CC chemokine MIP-1 beta can function as a monomer and depends on Phe13 for receptor binding, *Biochemistry 39*, 3401−3409.
53. Kim, S., Jao, S., Laurence, J. S., and LiWang, P. J. (2001) Structural comparison of monomeric variants of the chemokine MIP-1beta having differing ability to bind the receptor CCR5, *Biochemistry 40*, 10782−10791.
54. Pakianathan, D. R., Kuta, E. G., Artis, D. R., Skelton, N. J., and Hebert, C. A. (1997) Distinct but overlapping epitopes for the interaction of a CC-chemokine with CCR1, CCR3 and CCR5, *Biochemistry 36*, 9642−9648.
55. Wells, T. N., Power, C. A., Lusti-Narasimhan, M., Hoogewerf, A. J., Cooke, R. M., Chung, C. W., Peitsch, M. C., and Proudfoot, A. E. (1996) Selectivity and antagonism of chemokine receptors, *J. Leukocyte Biol. 59*, 53−60.
56. Forssmann, U., Hartung, I., Balder, R., Fuchs, B., Escher, S. E., Spodsberg, N., Dulkys, Y., Walden, M., Heitland, A., Braun, A., Forssmann, W. G., and Elsner, J. (2004) *n*-Nonanoyl-CC chemokine ligand 14, a potent CC chemokine ligand 14 analogue that prevents the recruitment of eosinophils in allergic airway inflammation, *J. Immunol. 173*, 3456−3466.
57. Rajarathnam, K., Sykes, B. D., Kay, C. M., Dewald, B., Geiser, T., Baggiolini, M., and Clark-Lewis, I. (1994) Neutrophil activation by monomeric interleukin-8, *Science 264*, 90−92.
58. Paolini, J. F., Willard, D., Consler, T., Luther, M., and Krangel, M. S. (1994) The chemokines IL-8, monocyte chemoattractant protein-1, and I-309 are monomers at physiologically relevant concentrations, *J. Immunol. 153*, 2704−2717.
59. Mantel, C., Kim, Y. J., Cooper, S., Kwon, B., and Broxmeyer, H. E. (1993) Polymerization of murine macrophage inflammatory protein 1 alpha inactivates its myelosuppressive effects in vitro: the active form is a monomer, *Proc. Natl. Acad. Sci. U.S.A. 90*, 2232−2236.
60. Avalos, B. R., Bartynski, K. J., Elder, P. J., Kotur, M. S., Burton, W. G., and Wilkie, N. M. (1994) The active monomeric form of macrophage inflammatory protein-1 alpha interacts with high- and low-affinity classes of receptors on human hematopoietic cells, *Blood 84*, 1790−1801.
61. Kim, K. S., Rajarathnam, K., Clark-Lewis, I., and Sykes, B. D. (1996) Structural characterization of a monomeric chemokine: monocyte chemoattractant protein-3, *FEBS Lett. 395*, 277−282.
62. Baggiolini, M. (1998) Chemokines and leukocyte traffic, *Nature 392*, 565−568.
63. Kraulis, P. J. (1991) MOLSCRIPT: a program to produce both detailed and schematic plots of protein structures, *J. Appl. Crystallogr. 24*, 946−950.
64. POV-Team (1997) Persistence of Vision Ray Tracer v3.02, World Wide Web, http://www.povray.org.

BI700936W